Prediction Accuracy of a Novel Dynamic Structure–Function Model for Glaucoma Progression

Rongrong Hu,[1,2] Iván Marín-Franch,[3] and Lyne Racette[2]

[1]Department of Ophthalmology, First Affiliated Hospital, College of Medicine, Zhejiang University, Hangzhou, China
[2]Indiana University, Eugene and Marilyn Glick Eye Institute, Indianapolis, Indiana, United States
[3]Departamento de Óptica, Facultad de Física, Universitat de València, Burjassot, Spain

Correspondence: Lyne Racette, Eugene and Marilyn Glick Eye Institute, Department of Ophthalmology, Indiana University, 1160 W Michigan Street, Indianapolis, IN 46202; lracette@iupui.edu.

Submitted: June 1, 2014
Accepted: October 14, 2014

Citation: Hu R, Marín-Franch I, Racette L. Prediction accuracy of a novel dynamic structure–function model for glaucoma progression. *Invest Ophthalmol Vis Sci*. 2014;55:8086–8094. DOI:10.1167/iovs.14-14928

Purpose. To assess the prediction accuracy of a novel dynamic structure–function (DSF) model to monitor glaucoma progression.

Methods. Longitudinal data of paired rim area (RA) and mean sensitivity (MS) from 220 eyes with ocular hypertension or primary open-angle glaucoma enrolled in the Diagnostic Innovations in Glaucoma Study or the African Descent and Glaucoma Evaluation Study were included. Rim area and MS were expressed as percent of mean normal based on an independent dataset of 91 healthy eyes. The DSF model uses centroids as estimates of the current state of the disease and velocity vectors as estimates of direction and rate of change over time. The first three visits were used to predict the fourth visit; the first four visits were used to predict the fifth visit, and so on up to the 11th visit. The prediction error (PE) was compared to that of ordinary least squares linear regression (OLSLR) using Wilcoxon signed-rank test.

Results. For predictions at visit 4 to visit 7, the average PE for the DSF model was significantly lower than OLSLR by 1.19% to 3.42% of mean normal. No significant difference was observed for the predictions at visit 8 to visit 11. The DSF model had lower PE than OLSLR for 70% of eyes in predicting visit 4 and approximately 60% in predicting visits 5, 6, and 7.

Conclusions. The two models had similar prediction capabilities, and the DSF model performed better in shorter time series. The DSF model could be clinically useful when only limited follow-ups are available. (ClinicalTrials.gov numbers, NCT00221923, NCT00221897.)

Keywords: computational modeling, structure–function, glaucoma progression

Glaucoma is a group of progressive optic neuropathies that have in common the chronic progressive degeneration of retinal ganglion cells (RGCs) and their axons. This degeneration results in distinctive changes in the structure of the optic nerve head and retinal nerve fiber layer, with associated visual field loss.[1] Histological studies have shown the existence of a relationship between the number of RGCs and visual function in both monkeys[2–4] and humans.[5,6] Similarly, clinical observations in glaucoma patients have shown correlations between structure and function.[7–9] Although multiple quantitative models have been developed to describe the association between structure and function in glaucoma,[10–13] the strength and nature of this relationship are not yet fully understood.[14] Initial studies suggested that structure and function were best defined by a curvilinear relationship.[15–17] More recent studies have demonstrated that the structure–function relationship may be linear when both measurements are expressed in linear units.[7,13,18] In addition, structure–function relationships have been shown to be influenced by sample composition (e.g., glaucoma severity),[19–21] units of measurements,[7,21,22] measurement variability,[23] and statistical methods.[22]

Although structural loss has been reported to be detectable before functional loss in glaucoma,[6,14,24–26] many studies show that functional loss can also be detected before structural loss.[2,6,14,24,25,27] Results from several large clinical trials show that structural changes can be detected before recognizable functional changes in some patients, while in others, glaucomatous functional loss appears without detectable structural changes.[28–30] Given that structural and functional measurements may each provide unique information about the presence of the disease and its progression, it may be useful to use both jointly to monitor glaucoma with a model that makes no strong assumptions about its development.

Several approaches have been developed to combine structural and functional measurements to detect glaucoma progression. The combination of structural and functional data using machine learning classifiers may improve diagnostic accuracy and detection of progression in comparison with human observers and/or current automated techniques.[31] Nevertheless, a recent study with machine learning classifiers showed that including both structural and functional measurements to assess progression did not provide better diagnostic power than including structural measurements alone.[32] Bayesian models that combine structural and functional measurements provide promising ways to improve the estimates of glaucoma progression.[33–35] In the present study, we propose a novel dynamic structure–function (DSF) model that uses structural and functional data jointly and that may be used as an intuitive graphical tool to monitor glaucoma progression in clinical practice. We test the predictive capability of the DSF model against that of ordinary least squares linear regression

(OLSLR), which has been commonly used to assess glaucoma progression.[36–38]

Methods

Participants

The study included 220 eyes of 150 subjects selected from the Diagnostic Innovations in Glaucoma Study (DIGS, 69 eyes of 52 subjects) and the African Descent and Glaucoma Evaluation Study (ADAGES, 151 eyes of 98 subjects). The DIGS and ADAGES studies have been described in detail elsewhere.[39] In brief, these ongoing longitudinal studies are prospectively designed to assess structure and function in glaucoma. These multicenter studies were approved by all appropriate Institutional Review Boards, adhered to the tenets of the declaration of Helsinki for research involving human subjects, and were performed in conformity with the Health Insurance Portability and Accountability Act (HIPAA).

All participants underwent a comprehensive ophthalmic examination, including review of medical history, best-corrected visual acuity, slit-lamp biomicroscopy, intraocular pressure (IOP) measurement, gonioscopy, and dilated funduscopic examination. The studies required at least one good-quality stereoscopic photograph and one reliable static automated perimetry (SAP) at baseline. All participants had open angles, best-corrected acuity of 20/40 or better, spherical refraction within 5.0 diopters, and cylinder correction within 3.0 diopters. Participants were excluded if they had a history of intraocular surgery (except for uncomplicated cataract surgery); secondary causes of glaucoma (e.g., iridocyclitis, trauma); other systemic or ocular diseases known to affect the visual field (e.g., pituitary lesions, demyelinating diseases, human immunodeficiency virus positive or acquired immune deficiency syndrome, or diabetes); medications known to affect visual field sensitivity; an inability to perform visual field examinations reliably; or life-threatening diseases.

Inclusion Criteria for the Present Study

The current study included participants with ocular hypertension (OHT, 68 eyes, 30.9%) or primary open-angle glaucoma (POAG, 152 eyes, 69.1%) classified at baseline. Among the POAG eyes, some eyes had glaucomatous optic neuropathy only (56 eyes, 25.5%); some eyes had abnormal visual field test result only (37 eyes, 16.8%), while others had both abnormal visual field test result and glaucomatous optic neuropathy (59 eyes, 26.8%). The classification criteria for each category have been reported by Sample et al.[39] In each structure–function data pair (considered as a visit), the structural measurement was performed within 1 month of the functional measurement. A minimum of 3 months separated each pair of structure–function data. All the eyes had at least 11 longitudinal structure–function data pairs. If eyes had more than 11 visits, we included the first 11 visits.

Structural Measures

Imaging of the optic disc was obtained by confocal scanning laser ophthalmoscopy with the Heidelberg Retina Tomograph II (HRTII, software version 3.1; Heidelberg Engineering, Heidelberg, Germany). The HRT software acquires three individual images for each eye during the initial scanning, from which it automatically computes a mean topography image. An experienced technician outlined the optic disc margin on the mean topography image while viewing simultaneous stereophotographs of the optic disc.[39] Only the images with mean pixel height standard deviation less than 50 μm were used, based on the recommendation of the manufacturer.[40]

Visual Function Measures

We included the results from SAP tests taken with the 24-2 pattern and Swedish interactive thresholding algorithm[41] on the Humphrey Field Analyzer (Carl Zeiss Meditec, Dublin, CA, USA). All visual fields were evaluated by the Visual Field Assessment Center at the Department of Ophthalmology, University of California-San Diego.[42] Unreliable visual fields, defined as more than 33% fixation losses, false-negative responses, and false-positive responses, were excluded. Visual fields with artifacts (e.g., lid and lens rim artifacts, fatigue effects) were also excluded. The two locations above and below the blind spot were excluded. The sensitivities in decibels (dB) at each of the remaining 52 test locations were first converted to the linear scale in 1/Lambert (1/L)[18] and then averaged to obtain the mean sensitivity (MS) value. The rationale for converting from logarithmic to linear units before averaging has been outlined by Hood et al.[43]

Conversion of Units for Structural and Functional Measurements

To quantify the structural and functional measurements in a comparable scale for the DSF model, the rim area (RA) and MS were expressed as percent of mean normal.[44,45] Mean normal values were 1112.63 1/L for MS and 1.44 mm^2 for RA, as calculated from an independent dataset of 91 eyes from 91 healthy subjects.[21] We calculated the percent of mean normal by scaling the values obtained for each eye using this sample of normal eyes as a reference; the values after the conversion could therefore be larger than 100% for some eyes. We can also convert these values from percent of mean normal to 1/L for MS and to mm^2 for RA through a simple rescaling. For example, a rate of change of –5% of mean normal per year would correspond to a rate of change of $-5/100 \times 1112.63 = -55.63$ 1/L per year and of $-5/100 \times 1.44 = -0.072$ mm^2 per year.

Dynamic Structure–Function Model

The DSF model quantifies the structural and functional changes over time and is presented with two descriptors, a centroid and its velocity vector. Figure 1 illustrates the DSF model in a two-dimensional space with MS on the *x*-axis and RA on the *y*-axis. The centroid is the central location of the longitudinal paired structural and functional measurements and is an estimate of the current stage of the disease. If vision of an average eye were intact, the centroid would be in the upper right corner of the two-dimensional plot, with approximately 100% of mean normal values for MS and RA. If all vision were lost, the centroid would be in the lower left corner of the plot, with 0% of mean normal MS and a percentage of mean normal RA corresponding to the residual tissue composed of glial and other nonretinal ganglion cells.[10] In the hypothetical example presented in Figure 1, the patient currently has approximately 50% of mean normal RA and MS (as shown by the latest centroid $\bar{X}_4$). The velocity vector describes the direction and rate at which the RA and MS are jointly changing over time. The velocity vector may point toward one of the four quadrants labeled Q1 to Q4. When the velocity vector points toward the third quadrant (Q3), there is observed worsening in both structure and function. Worsening can also be observed on structure only (vector pointing toward Q4) or function only (vector pointing toward Q2). Velocity vectors pointing toward Q1 indicate observed improvement in both structure and function. In addition to their direction, the length of the

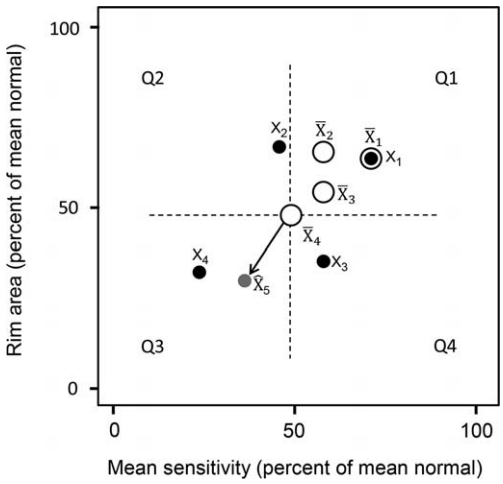

FIGURE 1. An illustration of the dynamic structure–function (DSF) model is presented. Four longitudinal paired measurements of rim area and mean sensitivity for a subject (*black solid circles*, labeled from X_1 to X_4) are plotted in a two-dimensional space showing structural and functional values. Structural and functional measurements are expressed in percent of mean normal, which could be greater than 100% in an individual eye. In the DSF model, the centroid (*empty circles*, labeled from $\bar{X}_1$ to $\bar{X}_4$) is an estimate of the current stage of the disease. The velocity vector (*arrow*) describes the direction and rate at which structure and function are jointly changing over time. The velocity vector may point toward any of the four quadrants (labeled from Q1 to Q4 in counterclockwise order). Q1, observed improvement on both RA and MS; Q2, observed worsening of MS and improvement of RA; Q3, observed worsening in both RA and MS; Q4, observed worsening of RA and improvement of MS. Based on the last centroid $\bar{X}_4$ and an estimated velocity vector, the future state (*gray solid circle* labeled $\hat{X}_5$) can be predicted.

velocity vectors provides visual information about the rate of glaucoma progression, with short vectors indicating slower progression and long vectors indicating faster progression.

The DSF model makes no assumption about the nature of the associations between structure and function (e.g., linear or nonlinear). And unlike previously presented models that take structure as a prior or give it more weight for early glaucoma, equal importance is given to both the structural and functional measurements in the DSF model. Based on the latest centroid and velocity vector, the expected observations at the next visit can be predicted (gray circle in Fig. 1) in the DSF model. Details for the implementation of the descriptive and predictive parts of the DSF model are presented in the Appendix.

Statistical Analysis

For each eye, paired longitudinal RA and MS data from the first three visits were used to predict the RA and MS at visit 4 with the DSF model. Then data from the first four visits were used to predict RA and MS at visit 5, and so on until predictions for visit 11 were obtained. Predictions for the fourth to 11th visits were also obtained with the OLSLR model by fitting OLSLR separately to RA and MS over time. Accordingly, there were a total of eight predictions for each eye with each model.

The prediction accuracy of the OLSLR and DSF models was assessed by the magnitude of the prediction error (PE, in percent of mean normal) defined as the L2-norm of the vector of differences between predicted values and actual measurements, that is, the square root of the sum of the squared differences for each dimension. The Wilcoxon signed-rank test was used to determine whether differences in PE between the OLSLR and DSF models were statistically significant. A similar analysis, comparing root-mean-square prediction error for series of visits, was performed by Russell et al.[35] All analyses were carried out in R,[46] SPSS (version 20.0; IBM, Armonk, NY, USA), and Igor Pro (version 6.34A; WaveMetrics, Portland, OR, USA). The R package visualFields[47] was used to process the visual field data.

TABLE. Characteristics of Study Sample at Baseline

	Mean	Median	First Quartile	Third Quartile
RA, mm²	1.25	1.23	1.03	1.44
MD, dB	−2.34	−1.14	−3.24	−0.02
Follow-up period, y	8.4	8.1	7.5	9.0
Intervals between visits, mo	11.0	10.1	6.6	13.2

MD, mean deviation.

RESULTS

The mean age of the 150 subjects included in this study was 58.8 with a standard deviation of 9.5 years at baseline. Eighty subjects (53.3%) were female. The Table shows the mean, median, and first and third quartiles for the structural and functional data at baseline, the follow-up period, and the intervals between visits.

Figure 2 shows comparisons in the PE between the OLSLR and DSF models at each visit. The PE obtained with the DSF model were, on average, significantly lower than with the OLSLR for the predictions of the fourth, fifth, sixth, and seventh visits by 3.42%, 1.70%, 1.19%, and 2.37% of mean normal, respectively ($P < 0.0001$ in predicting the fourth to sixth visits; $P = 0.02$ in predicting the seventh visit). There were no significant differences in predicting the eighth and

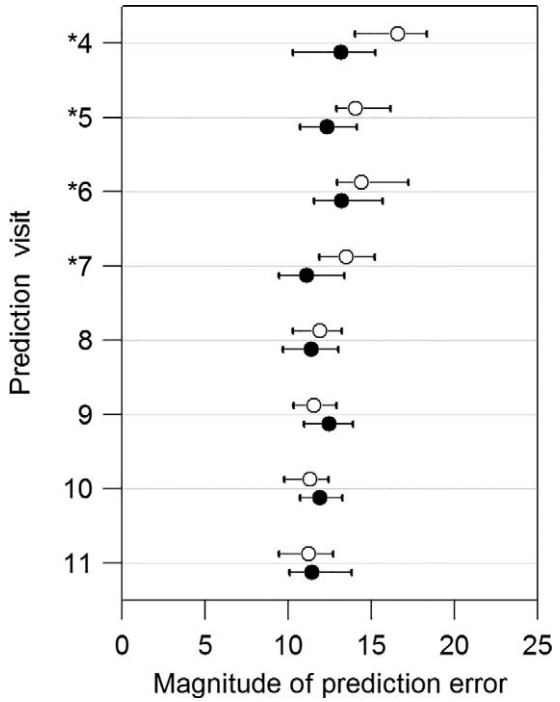

FIGURE 2. Comparisons of prediction errors in predicting RA and MS for visit 4 to visit 11. The *empty* and *solid circles* represent the median PE with the OLSLR and the DSF model, respectively. The *horizontal bars* show the 95% confidence intervals for the median PE. The *asterisks* denote the significant differences between the OLSLR and the DSF model based on Wilcoxon signed-rank test.

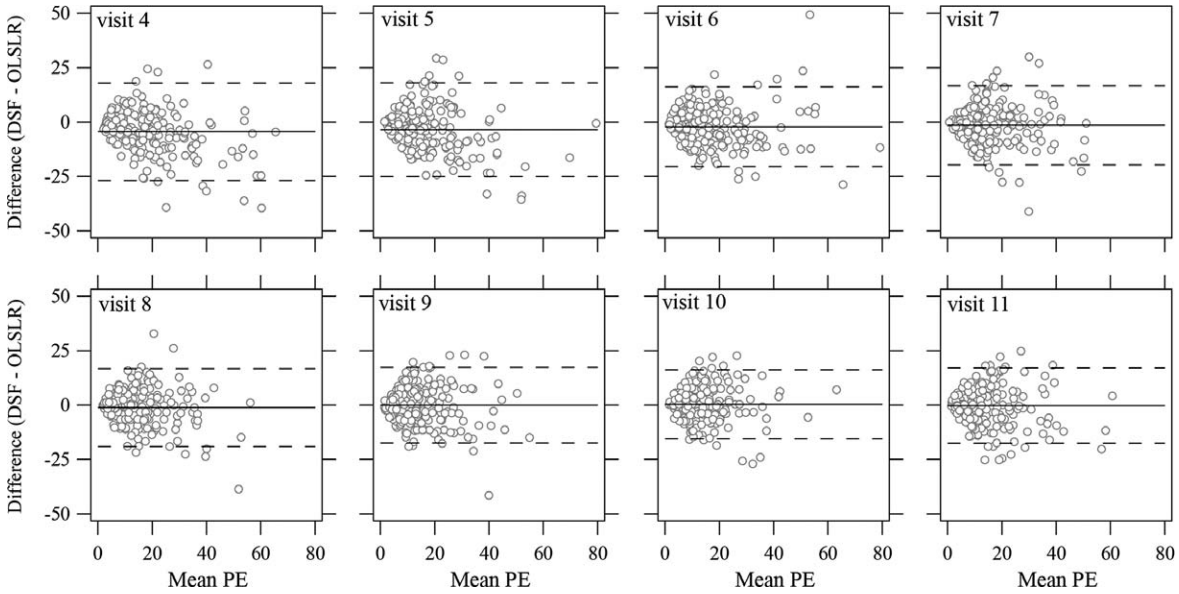

FIGURE 3. Limits of agreement between the OLSLR and the DSF model on the prediction errors for visit 4 to visit 11. The *horizontal axis* shows the mean PE of the OLSLR and DSF model for each eye. The *vertical axis* shows the PE difference calculated by the DSF model minus the OLSLR model. The *solid lines* and the *dashed lines* represent the mean difference and corresponding 95% limits of agreement. Six eyes (four eyes with an absolute difference in PE larger than 50% of mean normal and two eyes with a mean PE larger than 80% of mean normal) are not shown for clarity, but they were used in the calculation of the limits of agreement.

subsequent visits. As shown in Figure 2, both the OLSLR and DSF model showed a trend toward improved prediction accuracy with longer follow-up, as more data become available. For the prediction of the RA and MS for the fourth visit given a series of three visits, the DSF model performed better than OLSLR in 70% of the 220 eyes. For the predictions of RA and MS for the fifth, sixth, and seventh visits, the DSF model performed better than the OLSLR on approximately 60% of the eyes (range, 58.64%–60.45%). For predictions of the eighth to 11th visits, this ratio was close to 50% (range, 49.09%–51.82%).

Figure 3 shows mean-difference plots of the predictions between the OLSLR and DSF models. Even though performance of the DSF model was significantly better up to the prediction for visit 7, Figure 3 shows that these differences were not very large. Across all series, the absolute difference of PE between the two models were smaller than 10% of mean normal for more than 70% of the eyes (range from 70.91% in predicting visit 5 to 80.45% in predicting visit 8). There was slightly better agreement when more observations were available (see dashed lines in Fig. 3 that represent the limits of agreement).

Discussion

The ability to detect glaucoma progression when only limited follow-up examinations are available is clinically useful. We developed a novel model that describes glaucoma progression using longitudinal structural and functional data jointly, and we assessed its prediction accuracy on 220 eyes with OHT or POAG. On average, the DSF model provided significantly more accurate predictions for up to the seventh visit compared to the OLSLR model. For longer follow-up periods, the two models had similar prediction accuracy.

The European Glaucoma Society recommends that a minimum of six tests over 2 years be taken for newly diagnosed glaucoma patients to monitor early progression, and the current Humphrey Field Analyzer requires at least five visual field tests to perform the progression analysis.[48] In clinical practice, it is not always possible to obtain sufficiently long follow-up series due to either limited time or financial resources. Moreover, early detection of progression can help make early clinical decisions that might help reduce vision loss in some patients. In the present study, we showed that the DSF model performed better than the OLSLR, on average, for the first three to six visits, with approximately 60% to 70% of the eyes having more accurate prediction with the DSF model.

The DSF model provides an intuitive graphical representation of the current status of the disease and its progression. This representation could help clinicians to engage their patients in a conversation about their disease and allow them to effectively convey the progression information of the disease. As mentioned in Methods, velocity vectors that point toward the third quadrant (Q3) indicate observed progression on both structure and function. Velocity vectors that point toward either Q4 or Q2 indicate either worsening in structure with improvement in function or worsening in function with improvement in structure as captured by the structural and functional indices, respectively. Velocity vectors pointing toward Q1 indicate that both indices are improving. An increasing trend in visual function can be due to learning effects.[49] An increasing trend in structural indices can be due to reversal changes in optic nerve head owing to, for example, a reduction in the IOP,[50] although any pattern can be the result of test–retest variability.

Examples of prediction with the OLSLR and the DSF models are shown in Figure 4. For each subject, one prediction was selected with a short time series and another with a longer one. Subjects 1 and 2 were classified as POAG with both abnormal visual field test result and glaucomatous optic neuropathy at baseline. For subject 1, the DSF model provided more accurate predictions than the OLSLR for both visit 5 and visit 8. At visit 5, the OLSLR mainly overestimated the RA progression compared to the actual measurement. The prediction accuracy of OLSLR improved when the first seven visits were used to predict the eighth visit. For subject 2, who seems to have a rapid deterioration in visual sensitivity, the DSF model underestimated functional progression at both visit 5 and visit 10, whereas the OLSLR made more accurate

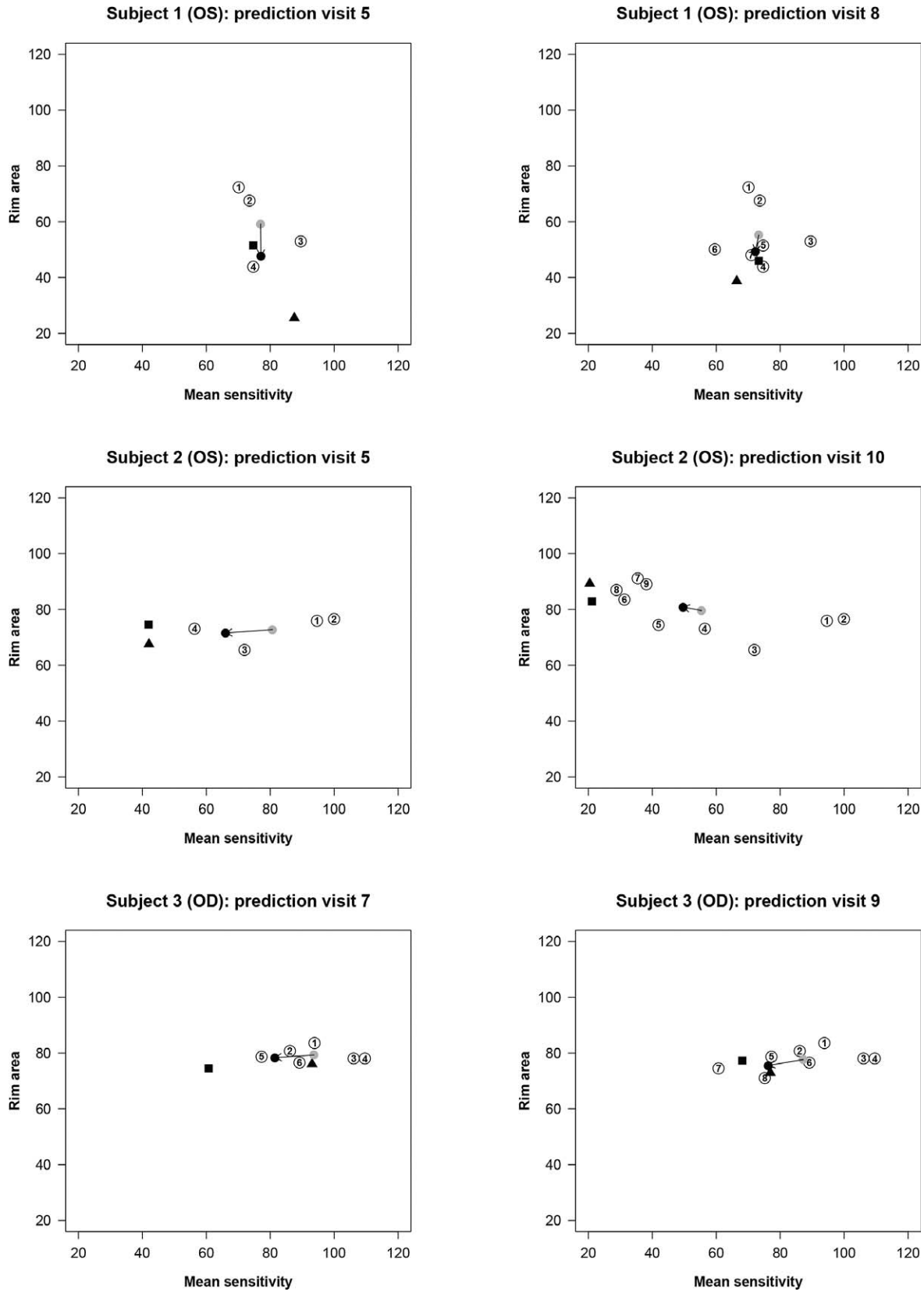

FIGURE 4. Patient examples with the OLSLR and the DSF models based on series of RA and MS measurements. In each part of the figure, paired RA and MS data are plotted as *circles* coded with the numbers that identify the chronological order of the visits. The *black triangle* represents the predicted RA and MS measurements with the OLSLR model. The *gray circle* represents the latest centroid, and the *black circle* represents the predicted RA and MS measurements with the DSF model, respectively. The *arrow* shows the vector of change connecting the latest centroid and the predicted measurements in the DSF model. The predictions of the OLSLR and DSF models are compared with the actual RA and MS measurements at that future visit (*black square*).

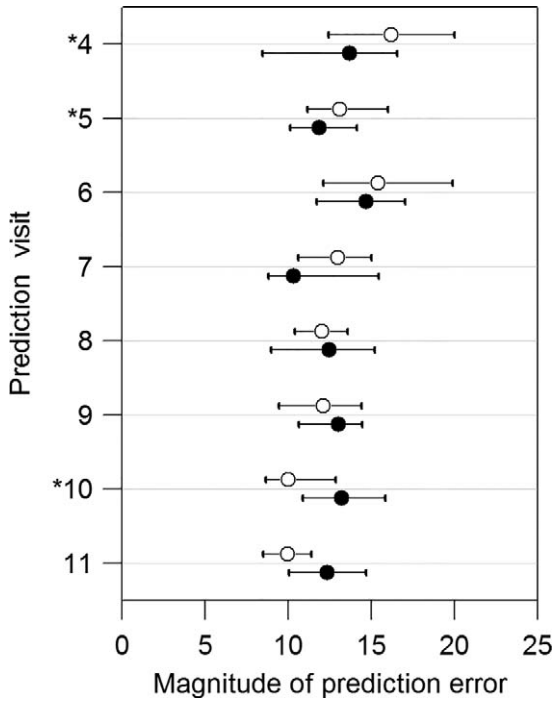

FIGURE 5. Comparisons of prediction errors for visit 4 to visit 11 in the subset of 94 eyes that are progressing significantly according to OLSLR. The *empty* and *solid circles* represent the median PE with the OLSLR and the DSF model, respectively. The *horizontal bars* show the 95% confidence intervals for the median PE. The *asterisks* denote the significant differences between the OLSLR and the DSF model based on Wilcoxon signed-rank test.

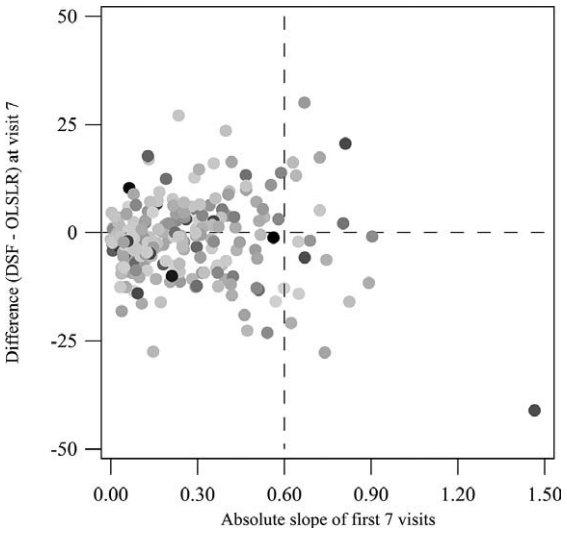

FIGURE 6. Analysis of the impact of the magnitude of changes observed over time on the differences in PE between the DSF model and OLSLR for 220 eyes. The absolute values of the slope of MS using OLSLR (in percent of mean normal per month) for the first seven visits are plotted on the *x*-axis, and the differences in PE between the DSF model and OLSLR at visit 7 are plotted on the *y*-axis. Each *dot* is *shaded* according to the magnitude of the absolute values of the slope of RA using OLSLR for the first seven visits: *Light shades* represent shallower slopes and *dark shades* represent steeper slopes.

predictions. Remarkably, the RA showed an improvement from visit 3, while there was a clear reduction in function. Worsening in function with improvement in structure is an observation that is not often reported in the literature. Subject 3 was classified as an OHT patient at baseline. For subject 3, the DSF model provided comparatively closer prediction than the OLSLR given a series of six visits, and there was little difference between the two models in predicting visit 9.

Because the DSF model is based on centroids calculated from all visits, there is a higher risk of making more conservative predictions for increasingly longer series of visits. This is noticeable for subject 2 (prediction at visit 10) in Figure 4 where the latest centroid has a higher MS than any of the most recent five observed measurements used for prediction and lower RA than any of the most recent four observed measurements. Yet the direction of change is well captured by the model. The model may underestimate the amount of change in progressing eyes increasingly when larger series of visits are taken into consideration.

To assess the impact of underestimation of the DSF model in progressing eyes with respect to the OLSLR, we selected a subset of 94 eyes that showed progression defined as a significant negative slope over the 11 visits using OLSLR ($P < 0.05$). Other definitions of progression could be used, but this one biases, if anything, the results toward OLSLR and against the DSF model we are assessing. With this progression criterion, 10 eyes showed progression on both RA and MS; 51 eyes showed progression on RA only; and 33 eyes showed progression on MS only. Figure 5 shows that the DSF model has significantly better prediction accuracy than OLSLR in predicting visits 4 and 5 and similar prediction accuracy in predicting all other visits, with the exception of visit 10, for which OLSLR was significantly better. This finding is not surprising in light of the facts that OLSLR provides unstable predictions for short series of visits, and that the predictions of the DSF model become increasingly conservative with longer series. Gardiner et al.[51] showed that trend analyses applied to short series (between six and nine visual field tests) was better to monitor progression compared to longer series (24 visual field tests) when the rate of change is not constant throughout the series. Nevertheless, here we show that the DSF model has better prediction accuracy than OLSLR in shorter series. Because early detection of progression is important clinically, improved prediction accuracy in short series for progressing eyes is a valuable advantage of the DSF model.

We further tested whether OLSLR made closer predictions than the DSF model as the magnitude of changes in MS and RA (absolute values of slopes) increased. As shown in Figure 6, no systematic differences are evident in the difference in the PE between the DSF model and OLSLR as a function of the magnitude of changes. In eyes with the largest magnitude of MS change (slopes greater than 0.6% of mean normal per month), the DSF model made better predictions than OLSLR in 11 eyes, whereas OLSLR made better prediction than the DSF model in seven eyes.

In any model that combines structural and functional measurements, it is necessary to use a common scale. In our study, the PE summarizes the error in structural and functional measurements and thus requires that both have comparable units. Percent of mean normal has been used in previous studies.[44,45] It is a relative scale, and the anchor points for both structure and function are the mean values based on a sample of healthy subjects.[21] For structure, a value of 10% of mean normal RA is not equivalent to 10% of RGCs, as other nonfunctional tissue surrounding ganglion cell bundles,[10] for example, the glial cells, forms part of the optic nerve head. Rim area can therefore be greater than zero even after all RGCs are lost. On the other hand, a value of 0% of mean normal MS is not equivalent to absolute blindness, but rather represents an inability to perceive the highest intensity that the perimeter is able to present. Percent of mean normal for MS would have

been very different if we had used a decibel scale instead of a linear scale. In our normative sample,[21] the mean normal MS was 30.46 dB, which corresponds to 1112.63 1/L. Therefore, in the linear scale, 50% of mean normal is 556.32 1/L and corresponds to 27.45 dB. For measurements lower than 10 dB, which are considered statutory blindness in the United States, the percent of mean normal using the linear scale would be 0.90% of mean normal, which is more representative than the corresponding 32.83% of mean normal using dB.

Teasing out true glaucomatous progression from variability is challenging. Both test–retest variability and between-subject differences can affect the determination of progression. In the context of the DSF model, between-subject differences can affect the location of the centroids, and test–retest variability can affect the direction and rate of change of the velocity vectors. Therefore, a vector of the same length pointing toward the same direction may indicate statistically significant progression in a patient with low test–retest variability and nonsignificant progression in a different patient with high variability. Hood et al.[23] reported that between-subject differences accounted for up to 87% and 71% of the total variance, respectively, in retinal nerve fiber layer thickness and visual field measurements for healthy subjects. Marín-Franch et al. (Marín-Franch I, et al. *IOVS* 2013;54:ARVO E-Abstract 2247) demonstrated that between-subject differences account for more dissociation between RA and MS than test–retest variability. Dissociation due to between-subject differences sets a strong limitation to the performance of any method that uses population statistics to assess glaucoma progression. In the present study, we assessed the prediction accuracy, but no significance test for progression is provided based on the DSF model. A natural next step in the development of the DSF model is to devise individualized statistical tests for glaucoma progression.

Since we used MS and RA, both the OLSLR and the DSF model could capture structural and functional deterioration due to aging.[52] For the purpose of comparing prediction accuracy of both models, age effects are unimportant; but for the clinical monitoring of glaucoma, it would be essential to have age-corrected structural and functional measures. Both models assume that the rate of change remains constant after the last observation, which can lead to errors, especially if we make predictions far in the future. For those subjects with two eyes eligible, we included both eyes for the analysis. To ensure that the possible correlation between the two eyes did not impact the results of the study, we replicated the analysis after selecting one eye at random for each subject and found similar results. In conclusion, the graphical description in a two-dimensional space provided by the centroid and the velocity vector of the DSF model allows for a more comprehensive view of glaucoma progression and may lead to further insights about its dynamics.

Acknowledgments

We thank the donors of National Glaucoma Research, a program of BrightFocus Foundation, for support of this research.

Supported also in part by an Indiana University–Purdue University Indianapolis Developing Diverse Researchers with InVestigative Expertise (DRIVE) award and by an unrestricted grant from Research to Prevent Blindness (Indianapolis, IN, USA). The DIGS and ADAGES studies were supported by National Institutes of Health Grants P30EY022589, EY021818, EY11008, U10EY14267, and EY019869; Eyesight Foundation of Alabama; Alcon Laboratories, Inc.; Allergan, Inc.; Pfizer, Inc.; Merck, Inc.; Santen, Inc.; Edith C. Blum Research Fund of the New York Glaucoma Research Institute (New York, NY, USA); and an unrestricted grant from Research to Prevent Blindness (New York, NY, USA). One of the authors (IM-F) developed the first drafts of the model under the NIH Grant EY007716 awarded to William H. Swanson.

Disclosure: **R. Hu**, None; **I. Marín-Franch**, None; **L. Racette**, None

References

1. Allingham RR, Damji KF, Freedman S, Moroi SE, Rhee DJ. *Shields' Textbook of Glaucoma*. 6th ed. Philadelphia, PA: Lippincott Williams & Wilkins; 2011:61–71, 92–100.
2. Harwerth RS, Carter-Dawson L, Shen F, Smith EL III, Crawford ML. Ganglion cell losses underlying visual field defects from experimental glaucoma. *Invest Ophthalmol Vis Sci*. 1999;40:2242–2250.
3. Harwerth RS, Crawford ML, Frishman LJ, Viswanathan S, Smith EL III, Carter-Dawson L. Visual field defects and neural losses from experimental glaucoma. *Prog Retin Eye Res*. 2002;21:91–125.
4. Harwerth RS, Carter-Dawson L, Smith EL III, Barnes G, Holt WF, Crawford ML. Neural losses correlated with visual losses in clinical perimetry. *Invest Ophthalmol Vis Sci*. 2004;45:3152–3160.
5. Quigley HA, Dunkelberger GR, Green WR. Retinal ganglion cell atrophy correlated with automated perimetry in human eyes with glaucoma. *Am J Ophthalmol*. 1989;107:453–464.
6. Kerrigan-Baumrind LA, Quigley HA, Pease ME, Kerrigan DF, Mitchell RS. Number of ganglion cells in glaucoma eyes compared with threshold visual field tests in the same persons. *Invest Ophthalmol Vis Sci*. 2000;41:741–748.
7. Garway-Heath DF, Holder GE, Fitzke FW, Hitchings RA. Relationship between electrophysiological, psychophysical, and anatomical measurements in glaucoma. *Invest Ophthalmol Vis Sci*. 2002;43:2213–2220.
8. Reus NJ, Lemij HG. Relationships between standard automated perimetry, HRT confocal scanning laser ophthalmoscopy, and GDx VCC scanning laser polarimetry. *Invest Ophthalmol Vis Sci*. 2005;46:4182–4188.
9. Schlottmann PG, De Cilla S, Greenfield DS, Caprioli J, Garway-Heath DF. Relationship between visual field sensitivity and retinal nerve fiber layer thickness as measured by scanning laser polarimetry. *Invest Ophthalmol Vis Sci*. 2004;45:1823–1829.
10. Hood DC, Kardon RH. A framework for comparing structural and functional measures of glaucomatous damage. *Prog Retin Eye Res*. 2007;26:688–710.
11. Harwerth RS, Wheat JL, Fredette MJ, Anderson DR. Linking structure and function in glaucoma. *Prog Retin Eye Res*. 2010;29:249–271.
12. Drasdo N, Mortlock KE, North RV. Ganglion cell loss and dysfunction: relationship to perimetric sensitivity. *Optom Vis Sci*. 2008;85:1036–1042.
13. Swanson WH, Felius J, Pan F. Perimetric defects and ganglion cell damage: interpreting linear relations using a two-stage neural model. *Invest Ophthalmol Vis Sci*. 2004;45:466–472.
14. Malik R, Swanson WH, Garway-Heath DF. "Structure-function relationship" in glaucoma: past thinking and current concepts. *Clin Experiment Ophthalmol*. 2012;40:369–380.
15. Airaksinen PJ, Drance SM, Douglas GR, Schulzer M. Neuroretinal rim areas and visual field indices in glaucoma. *Am J Ophthalmol*. 1985;99:107–110.
16. Jonas JB, Grundler AE. Correlation between mean visual field loss and morphometric optic disk variables in the open-angle glaucomas. *Am J Ophthalmol*. 1997;124:488–497.
17. Bartz-Schmidt KU, Thumann G, Jonescu-Cuypers CP, Krieglstein GK. Quantitative morphologic and functional evaluation of the optic nerve head in chronic open-angle glaucoma. *Surv Ophthalmol*. 1999;44(suppl 1):S41–S53.

18. Garway-Heath DF, Caprioli J, Fitzke FW, Hitchings RA. Scaling the hill of vision: the physiological relationship between light sensitivity and ganglion cell numbers. *Invest Ophthalmol Vis Sci*. 2000;41:1774–1782.
19. Ajtony C, Balla Z, Somoskeoy S, Kovacs B. Relationship between visual field sensitivity and retinal nerve fiber layer thickness as measured by optical coherence tomography. *Invest Ophthalmol Vis Sci*. 2007;48:258–263.
20. Gonzalez-Hernandez M, Pablo LE, Armas-Dominguez K, de la Vega RR, Ferreras A, de la Rosa MG. Structure-function relationship depends on glaucoma severity. *Br J Ophthalmol*. 2009;93:1195–1199.
21. Racette L, Medeiros FA, Bowd C, Zangwill LM, Weinreb RN, Sample PA. The impact of the perimetric measurement scale, sample composition, and statistical method on the structure-function relationship in glaucoma. *J Glaucoma*. 2007;16:676–684.
22. Marín-Franch I, Malik R, Crabb DP, Swanson WH. Choice of statistical method influences apparent association between structure and function in glaucoma. *Invest Ophthalmol Vis Sci*. 2013;54:4189–4196.
23. Hood DC, Anderson SC, Wall M, Raza AS, Kardon RH. A test of a linear model of glaucomatous structure-function loss reveals sources of variability in retinal nerve fiber and visual field measurements. *Invest Ophthalmol Vis Sci*. 2009;50:4254–4266.
24. Chauhan BC, McCormick TA, Nicolela MT, LeBlanc RP. Optic disc and visual field changes in a prospective longitudinal study of patients with glaucoma: comparison of scanning laser tomography with conventional perimetry and optic disc photography. *Arch Ophthalmol*. 2001;119:1492–1499.
25. Strouthidis NG, Scott A, Peter NM, Garway-Heath DF. Optic disc and visual field progression in ocular hypertensive subjects: detection rates, specificity, and agreement. *Invest Ophthalmol Vis Sci*. 2006;47:2904–2910.
26. Medeiros FA, Alencar LM, Zangwill LM, Bowd C, Sample PA, Weinreb RN. Prediction of functional loss in glaucoma from progressive optic disc damage. *Arch Ophthalmol*. 2009;127:1250–1256.
27. Artes PH, Chauhan BC. Longitudinal changes in the visual field and optic disc in glaucoma. *Prog Retin Eye Res*. 2005;24:333–354.
28. Kass MA, Heuer DK, Higginbotham EJ, et al. The Ocular Hypertension Treatment Study: a randomized trial determines that topical ocular hypotensive medication delays or prevents the onset of primary open-angle glaucoma. *Arch Ophthalmol*. 2002;120:701–713, discussion 829–830.
29. Keltner JL, Johnson CA, Anderson DR, et al. The association between glaucomatous visual fields and optic nerve head features in the Ocular Hypertension Treatment Study. *Ophthalmology*. 2006;113:1603–1612.
30. Miglior S, Zeyen T, Pfeiffer N, et al. Results of the European Glaucoma Prevention Study. *Ophthalmology*. 2005;112:366–375.
31. Bowd C, Goldbaum MH. Machine learning classifiers in glaucoma. *Optom Vis Sci*. 2008;85:396–405.
32. Yousefi S, Goldbaum MH, Balasubramanian M, et al. Glaucoma progression detection using structural retinal nerve fiber layer measurements and functional visual field points. *IEEE Trans Biomed Eng*. 2014;61:1143–1154.
33. Medeiros FA, Leite MT, Zangwill LM, Weinreb RN. Combining structural and functional measurements to improve detection of glaucoma progression using Bayesian hierarchical models. *Invest Ophthalmol Vis Sci*. 2011;52:5794–5803.
34. Medeiros FA, Zangwill LM, Girkin CA, Liebmann JM, Weinreb RN. Combining structural and functional measurements to improve estimates of rates of glaucomatous progression. *Am J Ophthalmol*. 2012;153:1197–1205.
35. Russell RA, Malik R, Chauhan BC, Crabb DP, Garway-Heath DF. Improved estimates of visual field progression using bayesian linear regression to integrate structural information in patients with ocular hypertension. *Invest Ophthalmol Vis Sci*. 2012;53:2760–2769.
36. Bengtsson B, Heijl A. A visual field index for calculation of glaucoma rate of progression. *Am J Ophthalmol*. 2008;145:343–353.
37. Heijl A, Lindgren G, Olsson J. A package for the statistical analysis of visual fields. *Doc Ophthalmol Proc Ser*. 1987;49:153–168.
38. Viswanathan AC, Fitzke FW, Hitchings RA. Early detection of visual field progression in glaucoma: a comparison of PROGRESSOR and STATPAC 2. *Br J Ophthalmol*. 1997;81:1037–1042.
39. Sample PA, Girkin CA, Zangwill LM, et al. The African Descent and Glaucoma Evaluation Study (ADAGES): design and baseline data. *Arch Ophthalmol*. 2009;127:1136–1145.
40. Fingeret M, Flanagan J, Liebmann JM. *The Essential HRT Primer*. Oakland, CA: Jocoto Advertising; 2005:25.
41. Bengtsson B, Olsson J, Heijl A, Rootzen H. A new generation of algorithms for computerized threshold perimetry, SITA. *Acta Ophthalmol Scand*. 1997;75:368–375.
42. Racette L, Liebmann JM, Girkin CA, et al. African Descent and Glaucoma Evaluation Study (ADAGES): III. Ancestry differences in visual function in healthy eyes. *Arch Ophthalmol*. 2010;128:551–559.
43. Hood DC, Anderson SC, Wall M, Kardon RH. Structure versus function in glaucoma: an application of a linear model. *Invest Ophthalmol Vis Sci*. 2007;48:3662–3668.
44. Hot A, Dul MW, Swanson WH. Development and evaluation of a contrast sensitivity perimetry test for patients with glaucoma. *Invest Ophthalmol Vis Sci*. 2008;49:3049–3057.
45. Shafi A, Swanson WH, Dul MW. Structure and function in patients with glaucomatous defects near fixation. *Optom Vis Sci*. 2011;88:130–139.
46. R Core Team. *R: A language and environment for statistical computing*. Vienna, Austria: R Foundation for Statistical Computing; 2014.
47. Marín-Franch I, Swanson WH. The visualFields package: a tool for analysis and visualization of visual fields. *J Vis*. 2013;13:10:1–12.
48. European Glaucoma Society. *Terminology and Guidelines for Glaucoma*. 3rd ed. Savona, Italy: Editrice Dogma; 2008:86–87.
49. Heijl A, Bengtsson B. The effect of perimetric experience in patients with glaucoma. *Arch Ophthalmol*. 1996;114:19–22.
50. Park KH, Kim DM, Youn DH. Short-term change of optic nerve head topography after trabeculectomy in adult glaucoma patients as measured by Heidelberg retina tomograph. *Korean J Ophthalmol*. 1997;11:1–6.
51. Gardiner SK, Demirel S, De Moraes CG, et al. Series length used during trend analysis affects sensitivity to changes in progression rate in the ocular hypertension treatment study. *Invest Ophthalmol Vis Sci*. 2013;54:1252–1259.
52. Harwerth RS, Wheat JL, Rangaswamy NV. Age-related losses of retinal ganglion cells and axons. *Invest Ophthalmol Vis Sci*. 2008;49:4437–4443.

Investigative Ophthalmology & Visual Science

Appendix

The DSF model describes change in structure and function using estimates of the current state and of the direction and rate of change. The model can be split into two key parts: a descriptive part and a predictive part. The descriptive part is updated as more structural and functional observations become available and is the basis for the predictive part of the model.

Imagine that a subject who has already visited the clinic $k-1$ times comes back t_k months after the last visit. This patient has visited the clinic, on average, every

$$\bar{t}_k = \frac{1}{k-1}\sum_{i=2}^{k} t_i$$

months. The estimated present state, or centroid $\bar{x}_k$, can be estimated recursively from the estimated state at the previous visit and the present observation x_k as

$$\bar{x}_k = \frac{(k-1)\bar{x}_{k-1} + x_k}{k},$$

and the direction and rate of change, or velocity vector $\bar{v}_k$ can be estimated as

$$\bar{v}_k = \frac{1}{k\bar{t}_k}(x_k - \bar{x}_{k-1}).$$

The velocity vector in this model can be interpreted as the observed change in structure and function per month, but we could also express it as rate of change per year or decade if we expressed time between visits in those units. Given the centroid of the previous visit $\bar{x}_{k-1}$, the average time between visits up to visit $\bar{t}_k$, and velocity vector in the current visit $\bar{v}_k$, we can calculate the current centroid $\bar{x}_k$; thus

$$\bar{x}_k = \bar{x}_{k-1} + \bar{t}_k\bar{v}_k,$$

where the first centroid starts at the first observation (i.e., $\bar{x}_1 = x_1$), we take the reference time to be that of the first visit (i.e., $\bar{t}_1 = 0$), and we set $\bar{v}_1 = 0$. The rate of change $\bar{v}_k$ is updated from visit to visit, and hence it changes with the incorporation of each new visit.

To predict the state in the next visit $k+1$ after a period of time t_{k+1}, we need to provide an estimation of the velocity vector at $k+1$. Different approaches could be employed to provide this estimation, and the one we propose here is to first calculate all rates of change from visit to visit,

$$\hat{v}_i = \frac{x_i - x_{i-1}}{t_i}; i = 1, \ldots, k,$$

and to average them; thus,

$$\hat{v}_{k+1} = \frac{1}{k-1}\sum_{i=2}^{k}\hat{v}_i.$$

Although there is a lot of noise from visit to visit, this approach allows for the overall trend to be captured in the averaged velocity vector. The direction of the predicted vector is the average direction of all the historic changes from visit 1 to visit k weighted by the time lapse between visits. This vector of change is different from the velocity vector used if we wanted to predict the centroid at $k+1$, which can be calculated by dividing the vector of change by $k+1$, to account for the number of observations (plus the prediction). That is, $\hat{\bar{v}}_{k+1} = \hat{v}_{k+1}/(k+1)$.

Finally, since the average time between the $k+1$ visits is

$$\bar{t}_{k+1} = \frac{1}{k}[t_{k+1} + (k-1)\bar{t}_k],$$

we predict the structural and functional values $\hat{x}_{k+1}$ as

$$\hat{x}_{k+1} = \bar{x}_k + \bar{t}_{k+1}\hat{v}_{k+1}$$

The accuracy of the predicted value, $\hat{x}_{k+1}$, depends on the accuracy of estimates of current state and of the predicted vector of change, and relies on the assumption that both direction and rate remain unchanged between visits k and $k+1$.

Investigative Ophthalmology & Visual Science